# Reaction zones and quenched charged-particle systems with long-range interactions

A. D. Rutenberg
*Centre for the Physics of Materials, Physics Department, McGill University, 3600 rue University, Montréal, Quebec, Canada H3A 2T8*
(Received 30 April 1998)

We determine the evolving segregated or mixed morphology of charged-particle systems with long-range power-law interactions and overall charge neutrality that have been quenched to a low temperature. Segregated morphology systems are characterized by the size of uniformly charged domains, $L(t)$, the particle separation within the domains, $l_{AA}(t)$, the particle flux density leaving the domains, $J(t)$, the width of reaction zones between domains, $W(t)$, the particle spacing within the reaction zones, $l_{AB}(t)$, and the particle lifetime in the reaction zones, $\tau(t)$. Mixed morphology systems are essentially one large reaction zone, with $L \sim l_{AB} \sim l_{AA}$. By relating these quantities through the scaling behavior of particle fluxes and microscopic annihilation rates within reaction zones, we determine the characteristic time exponents of these quantities at late times. The morphology of the system, segregated or mixed, is also determined self-consistently. With this unified approach, we consider systems with diffusion and/or long-range interactions, and with either uncorrelated or correlated high-temperature initial conditions. Finally, we discuss systems with particlelike topological defects and electronic systems in various substrate dimensions—including quantum Hall devices with Skyrmions. [S1063-651X(98)09909-7]

PACS number(s): 82.20.Mj, 05.40.+j, 47.54.+r, 61.30.Jf

## I. INTRODUCTION

We consider reaction-diffusion systems without long-range interactions [1–8] that involve two diffusing species of particles which annihilate on contact, $A+B \rightarrow \varnothing$. The temperature is assumed to be low enough that the reverse reaction can be ignored, so that the densities at late times are determined by the disordered initial conditions. For equal initial mean densities of the particles and antiparticles, there are two known morphologies at late times [1]. The first, for spatial dimension $d \geqslant 4$, is a well mixed morphology in which mean-field dynamics applies to the particle density, $\partial_t \overline{\rho} = -C\overline{\rho}^2$. This leads to $\overline{\rho}(t) \sim 1/t$ at late times. The second, for $d<4$, is a segregated morphology consisting of single-species domains of characteristic size $L(t)$. The evolution is via diffusive currents feeding particles from the domains into reaction zones where they are annihilated by antiparticles. The evolution of the mean domain density, $\overline{\rho} \sim t^{-d/4}$, is easily demonstrated for $d>2$ if the two species have equal diffusion constants, so that the density difference $\Delta\rho \equiv \rho_A - \rho_B$ satisfies a linear diffusion equation [1,2]. This also applies more generally [3].

In the mixed morphology, initial charge fluctuations decay faster than the mean particle density, and can be ignored. In the segregated morphology, long-wavelength initial fluctuations decay more slowly and asymptotically determine the domain structure. In that case, the profile of the domains and the structure of the reaction zone can be understood through the particle fluxes and the annihilation kinetics of particle pairs [4–7], as well as on a more formal level [3].

It has been recognized from the beginning [1] that long-range interactions between oppositely charged particles and antiparticles change the evolution of a reaction-diffusion system—both by changing the initial charge-density fluctuations, and by changing the subsequent dynamics. However, progress has been gradual due to the greater complexity of long-range interactions both in analytical models [9] and in computer simulations, and by the need to understand the force-free case first. Nevertheless, progress in long-range models has been made along a number of fronts [10–18]. For systems with long-range interactions but no diffusion, and with uncorrelated initial conditions, Toyoki presented an analysis of a mixed morphology [10]. Complementing that work, Ispolatov and Krapivsky [11] considered segregated systems and simulated a variety of force-laws in $d=1$. For both long-range interactions and diffusion, with uncorrelated initial conditions, a self-consistent model by Ginzburg, Radzihovsky, and Clark [12] and a complementary scaling model [13] has captured the density evolution for $n \geqslant d-1$, where $n$ characterizes the force between particles via $f \sim r^{-n}$ [see Eq. (1) below]. The $n=d-1$ Coulombic case has also been treated by Ohtsuki [14]. High-temperature correlated initial conditions have also been discussed [15].

In this paper, we are interested in the late-time evolution of initially random distributions of charges in homogeneous systems with overall charge neutrality. We use the scaling behavior, with respect to length scale, of the initial charge fluctuations, the resulting large-scale currents, and the local annihilation rate of particles to determine both the morphology and the time exponents of the characteristic lengths. Our approach is based on the assumption that domain structures are characterized by only two lengths: their size $L(t)$ and their characteristic particle separation $l_{AA}(t)$, where the average density $\overline{\rho} \sim l_{AA}^{-d}$. This is comparable to the dynamical-scaling assumption of phase-ordering systems [19] and, with appropriate physical input, leads to a self-consistent description of the system evolution. Between the domains, we allow for reaction zones of width $W(t)$, within which both particle species are mixed with typical spacing $l_{AB}(t)$ and lifetime $\tau$. For segregated systems, charged currents are absorbed in the reaction zones. For mixed systems, the reaction zone pervades the system. Our approach of balancing currents with

 

annihilation within reaction zones is in the spirit of the treatment of force-free systems by Redner and Leyvraz [7]; and for these systems our results agree with the renormalization-group analysis of Lee and Cardy [3].

We ignore correlations apart from the characteristic lengths $l_{AA}$, $l_{AB}$, $L$, and $W$ which determine the densities and sizes of the domains and reaction zones. As a result, our approach is insensitive to early-time dynamics, unequal diffusion constants [20], and motion of domain boundaries. All of these factors help determine the *amplitude* of the growth laws. Nonetheless, from the scaling properties of currents and lengths we can extract the asymptotic time exponents. One benefit of our approach is that its conclusions are robust to the details of the system, and that it provides a vividly physical picture of the morphological evolution of charged systems with long-range interactions.

We should emphasize what is new in this paper. We do not assume which morphology the system selects, but determine it self-consistently from the physics. We treat a large number of different cases with the same unified approach, *including* the well understood diffusion-only systems. We determine the reaction-zone width and density, and also discover nontrivial domain-edge profiles. For uncorrelated initial conditions, we discover several regimes where ballistic annihilation is the dominant annihilation mechanism. For high-temperature equilibrium initial conditions, we determine the appropriate initial charge-fluctuation spectrum and show how it modifies the subsequent evolution and morphology of the system.

In Sec. II, we introduce long-range interactions with overdamped dynamics between initially random particles and antiparticles. For equilibrium initial conditions, we calculate the expected initial long-wavelength charge fluctuations, characterized by $\mu$ (Sec. II A; see also Fig. 1). From the charge fluctuations, using a scaling form for the domain profiles near edges, we determine the scaling of charged currents (Sec. II B; see also Table I and Fig. 2). We then consider various mechanisms of particle annihilation (Sec. II C; see also Figs. 3 and 4). We combine our results on currents and on annihilation, by balancing the currents with the annihilation rates in the reaction zones (Sec. II D). This is sufficient to determine both the system morphology and the time dependence of the domain size $L$ and of the average density, $\overline{\rho}$ (Fig. 5 and Table II). We next consider the reaction zone in more detail, and determine its width $W$ and particle spacing $l_{AB}$, as well as the typical lifetime $\tau$ within the reaction zone (Sec. II E; see also Table III). Finally we discuss our results, including implications for coarse-grained treatments (Sec. II F).

We discuss the previous reaction-diffusion literature (Sec. III), then discuss applying our results to electrically charged ($n=2$) systems in various substrate dimensions (Sec. IV). We emphasize that, for $d<3$, interesting new decay laws and segregated morphologies are found. We then discuss the application of our results to quenched phase-ordering systems with pointlike topological defects (Sec. V). We can also extend our approach to include Lévy superdiffusive systems, as well as subdiffusive systems (Sec. VI).

The effect of short-range cutoffs on the power-law interactions can easily be treated (Sec. VII). We numerically explore our results on domain profiles (Sec. VIII; see also Fig. 6). Finally, we conclude (Sec. IX).

Throughout this paper we concentrate on exponents, or scaling dependencies, of various quantities in the late-time limit. Inequalities apply to exponents, so that a process is dominant if it is asymptotically largest as $t\to\infty$. We denote the mechanisms with a subscript $D$, $F$, or $B$ for diffusive, local-force-driven, or long-range ballistic processes, respectively.

## II. LONG-RANGE INTERACTIONS

We work in the overdamped limit, in which particle velocity equals the applied force times a constant mobility, $\eta$. The pairwise forces are

$$f_{ij}=Cq_iq_j/r_{ij}^n \tag{1}$$

between particles with charges $\{q_i\}$ and pairwise separations $\{r_{ij}\}$. This corresponds to a pairwise interaction energy $E_{ij}=Cq_iq_jr_{ij}^{1-n}/(n-1)$, with a logarithm at $n=1$. Thus the particle velocity is

$$\partial_t\vec{r}_i=\eta\sum_{j\neq i} f_{ij}\hat{r}_{ij}+\vec{\phi}_i, \tag{2}$$

where we have added a random uncorrelated noise for diffusive motion with diffusion constant $D$, where $\langle\vec{\phi}_i(t)\cdot\vec{\phi}_j(t')\rangle=D\delta_{ij}\delta(t-t')$. When oppositely charged particles approach within a fixed capture radius $r_c$, they annihilate instantaneously [21]. We are interested in the behavior of the system at late times when distinct length scales are well separated.

### A. Initial conditions

Most studies of reaction diffusion with long-range interactions have focused on the case of random uncorrelated initial conditions, where the particles are randomly placed with a local Poisson distribution [10–14,16–18]. Experimentally, it is more natural to quench a system of charged particles from a high-temperature state in which they are in thermal equilibrium [1,15].

Charge fluctuations may be usefully characterized by the typical charge density at scale $L$,

$$\delta\rho\sim L^{-\mu}. \tag{3}$$

This can be thought of as the excess charge density in a region of size $L$ *after* coarse graining to that scale. It is also related to the magnitude of the Fourier component $\rho_{1/L}$ of the charge density by

$$|\rho_{1/L}|\sim L^{d/2-\mu}, \tag{4}$$

as obtained by summing up $O(L_\infty^d/L^d)$ uncorrelated contributions of size $L^d\delta\rho(L)$, and normalizing out the constant contribution due to the system size, $L_\infty$. As a result we can obtain $\mu$ directly from $\rho_k$.

We are only interested in the scale dependence of initial charge fluctuations that survive for long times—i.e., for fluctuations at large scales and correspondingly small $k$. Hence we consider a continuum charge density $\rho(r)$ with energy

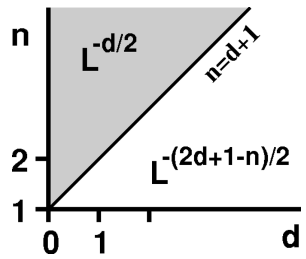


FIG. 1. Charge density fluctuations $\delta\rho \sim L^{-\mu}$ for equilibrated high-temperature initial conditions. In the shaded region the initial conditions are uncorrelated at large scales; in the unshaded region interactions reduce large-scale charge fluctuations.

$$E = \tilde{C}/2 \int d^d r d^d r' \rho(r)\rho(r')/|r-r'|^{n-1}$$

$$= \tilde{C}/2 \int \frac{d^d k}{(2\pi)^d} \rho_k \rho_{-k} \epsilon_k . \tag{5}$$

From $\epsilon_k \equiv \int d^d x e^{ik\cdot x} x^{1-n}$, we obtain $\epsilon_k = \pi^{d/2}(k/2)^{n-1-d}\Gamma[(d+1-n)/2]/\Gamma[(n-1)/2]$ for $1<n<d+1$. For $n \geqslant d+1$ we must introduce an UV cutoff, the inverse particle separation [22], which determines a leading $\epsilon_k = \text{const}$ small-$k$ behavior. For $n=1$ the interaction in Eq. (5) should be logarithmic, and we obtain $\epsilon_k = \pi^{d/2} 2^{d-1} k^{-d} \Gamma(d/2)$. Imposing equipartition on Eq. (5) with temperature $T$, we obtain $\langle \rho_k \rho_{-k} \rangle \sim k_B T/\epsilon_k$.

This derivation reproduces the small-$k$ behavior of a more complete variational approach; see, e.g., Ref. [23]. Entropy factors do not affect the leading long-wavelength fluctuations, so that the integrand in Eq. (5) is correct for small $k$. This means that $\rho_k$ is Gaussian distributed for $k \to 0$, and $\langle |\rho_k| \rangle \sim \epsilon_k^{-1/2}$. Comparing with Eq. (4), we obtain

$$\mu = \begin{cases} (2d+1-n)/2, & 1 \leqslant n < d+1 \\ d/2, & n > d+1. \end{cases} \tag{6}$$

This is illustrated in Fig. 1. Note that $d/2 \leqslant \mu \leqslant d$, so that long-range interactions always suppress initial charge fluctuations. The maximal suppression is achieved at $n=1$ when $\mu = d$. (For $n<1$, we expect higher-point correlations to be significant.) For sharp enough interactions, with $n > d+1$, we recover uncorrelated initial conditions with $\mu = d/2$.

The charge excess at scale $L$, as discussed above, is quite different from the charge excess within a sharp boundary of scale $L$, for example inside a sphere of radius $L$. The latter has been proposed as a measure of charge fluctuations, particularly in Coulombic systems in general dimensions, with $n = d-1$, where a Gauss's law applies (see, e.g., Refs. [1,15,16]) and in systems with topological defects [24–26] where similar integral identities apply to the topological charge density. At high temperatures the charge inside a given closed surface is proportional to the square root of the surface area, as obtained from integrating the appropriate random high-temperature field over the surface [26]. Taken literally, this would imply that $\mu = (d+1)/2$ [15], i.e., larger charge fluctuations than indicated in Eq. (6) for Coulombic interactions. However, a sharp surface picks up charge fluctuations at short scales *in addition to* the desired large-scale fluctuations. Indeed, the Coulombic or high-temperature nature of the system is moot—arbitrary *sharp* surfaces within a system with microscopic charge heterogeneities (e.g., atoms or thermal fluctuations) pick up charge fluctuations proportional to the square root of the surface area. Useful and appropriate charge fluctuations at scale $L$ are given by Eq. (6), and are not mixed with charge fluctuations at short scales [27].

### B. Domain profile and currents

Charge fluctuations, coarse grained to scales much larger than typical particle separations, decay via charged currents. These currents can be diffusive, or can be driven by the long-range interactions. We first consider segregated systems, where the domain size $L(t)$ sets the scale of surviving charge fluctuations. The average density within a domain, $\overline{\rho} \sim l_{AA}^{-d}$ is simply proportional to the initial fluctuations at the domain scale, $\delta\rho(L)$, so that [15]

$$L \sim l_{AA}^{d/\mu} . \tag{7}$$

Charge fluctuations at scales much larger than $L$ cannot have relaxed, since charge transport at larger scales is cut off by the domain structure. We now *assume* [28] that the domain profile is only determined by the average density $\overline{\rho}$ and size $L$ of domains. For example, domains have a typical density profile

$$\rho(r) = l_{AA}^{-d} f(r/L),$$

$$\sim l_{AA}^{-d} (r/L)^{\alpha}, \tag{8}$$

where $r$ is measured from the edge of the domain. The second equation holds near a domain edge, with $r \ll L$. We also require $r \gg W$, so that the profile is probed well away from the reaction zone. This scaling form was proposed by Leyvraz and Redner in diffusive systems [7], and was numerically confirmed in $d=1$.

The assumption of an invariant scaled domain morphology is powerful, and is sufficient to determine the coarse-grained current density $J$ near the domain edge. The flux must have a dominant nonzero constant contribution near the domain edge for $r \ll L$ arising from the evolution of domain density, since no annihilation takes place in the domain interior. Consider the net charge of a domain, $Q \sim L^d \overline{\rho} \sim L^{d-\mu}$. It implies a nonzero net flux density $J \sim \dot{Q}/L^{d-1} \sim L^{1-\mu}/t$ near the domain edge. The exponent characterizing the domain profile, $\alpha$, is constrained to allow the dominant $J$ to be finite but nonzero for $r/L \to 0^+$.

If the dominant current is diffusive, then $J_D \sim \overline{\rho}/L$, so that

$$J_D \sim L^{-(1+\mu)}. \tag{9}$$

Imposing a constant diffusive current condition at the domain edge implies a linear profile, with $\alpha = 1$. This agrees with studies of domain profiles in diffusive systems [7].

If the dominant current is driven by long-range forces, then it is given by the coarse-grained field times the local charge density, $J_F \sim \rho(r) F(r)$. The field $F(r)$ at a distance $r$ away from the domain edge due to the charge distribution given by Eq. (8) is

TABLE I. Domain profile exponents $\alpha$, coarse-grained field a distance $r \ll L$ from the domain edge $F(r)$, and force-driven flux $J_F$ for different interaction exponents $n$. When diffusive fluxes dominate, $\alpha = 1$.

| | $\alpha$ | $F(r)$ | $J_F$ |
|---|---|---|---|
| $n<d$ | 0 | $L^{d-n-\mu}$ | $L^{d-n-2\mu}$ |
| $d<n<d+1$ | $(n-d)/2$ | $r^{(d-n)/2}L^{(d-n-2\mu)/2}$ | $L^{d-n-2\mu}$ |
| $n>d+1$ | $d/(n+d-1)$ | $(L/r)^{d/(n+d-1)}L^{-(n+1)/2}$ | $L^{-(n+d+1)/2}$ |

$$F(r) \sim \int_{l_{AA}(r)}^{L} d^d x [\rho(r+x) - \rho(r-x)]/x^n. \qquad (10)$$

We have used the domain scale as the long-distance cutoff, and the local interparticle spacing $l_{AA}(r) \sim \rho(r)^{-1/d}$ as the short-distance cutoff. We also restrict the angular integral to be close to the normal direction from the interface, which retains the scaling behavior of $F(r)$ without requiring detailed information about the domain shape.

For $d>n$, charges at distances of order $L$ determine $F$, so that $F \sim \overline{\rho} L^{d-n} \sim L^{d-n-\mu}$. For a constant flux $J_F$ at small $r$, we must have $\rho(r) \sim$ const (i.e., $\alpha = 0$), so that $J_F \sim \overline{\rho^2} L^{d-n} \sim L^{d-n-2\mu}$. When $d>2n$, with uncorrelated initial conditions ($\mu = d/2$), $F$ increases with the upper cutoff of the integral in Eq. (10), so that we should use the *system size* $L_\infty$ rather than $L$. For this case, the system size enters the dynamics, and the thermodynamic limit does not exist [10,11].

For $d<n$, the local charge distribution dominates the $F(r)$ integral. We can expand the density for $x \ll r$, and find $F(r) \sim \rho(r)^{(n-1)/d} r^{-1}$ for $n>d+1$. For $d<n<d+1$, on the other hand, the integral is dominated by scales around $r$, and we find $F(r) \sim r^{\alpha+d-n}/[l_{AA}^d L^\alpha]$. Insisting that $J_F$ approaches a nonzero constant near the domain edge, we obtain Table I. These results apply far from the reaction zone, but otherwise close to the domain edge: $W \ll r \ll L$. (We determine the reaction-zone width in Sec. II E.) We see that currents dominantly driven by power-law interactions lead to nontrivial domain profiles, with $0 \leqslant \alpha \leqslant \frac{1}{2}$, in dramatic contrast to the diffusive case where $\alpha = 1$. It is also interesting that the current $J_F$ has a long-range form for $d<n<d+1$, even though $\alpha \neq 0$.

When both long-range forces and diffusive effects are present, then we must compare $J_F$ and $J_D$, and identify which is larger at late times. We summarize the results in Fig. 2 for random uncorrelated initial conditions. For equilibrated high-temperature initial conditions, $J_D$ is always asymptotically larger at late times.

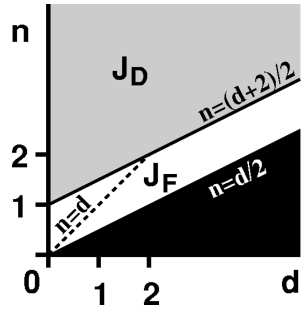


FIG. 2. The asymptotically dominant flux starting from uncorrelated initial conditions ($\mu = d/2$). When $J_F$ dominates, see Table I; when $J_D$ dominates, see Eq. (9). For equilibrated high-temperature initial conditions, $J_D$ always dominates at late times.

### C. Particle annihilation

In a well mixed region of the system, where the typical spacing between oppositely charged particles is $l_{AB}$, what is the scaling of the particle lifetime $\tau(l_{AB})$? There are three annihilation mechanisms: diffusive annihilation ($\tau_D$), local interaction-driven annihilation ($\tau_F$), and ballistic annihilation ($\tau_B$). We determine their scaling dependence on $l_{AB}$, and hence identify the dominant mechanism at late times. Our essentially microscopic approach also provides insight into the applicability of coarse-grained treatments (see Sec. II F).

In the force-free case, particles move diffusively with diffusion constant $D$, and annihilate with oppositely charged particles when they approach within a fixed distance $r_c$. In $d \leqslant 2$, trajectories are space filling and $\tau_D \sim l_{AB}^2/D$—the time it takes for a particle to diffuse $l_{AB}$. For $d>2$, $\tau_D \sim l_{AB}^d/(D r_c^{d-2})$, since each particle must explore the characteristic volume per particle to find an antiparticle to annihilate. We have

$$\tau_D \sim \begin{cases} l_{AB}^2, & d<2 \\ l_{AB}^d, & d>2. \end{cases} \qquad (11)$$

In the diffusion-free case, considering only local interactions $f \sim r^{-n}$ between two particles initially separated by $l_{AB}$, the annihilation time

$$\tau_F \sim l_{AB}^{n+1}. \qquad (12)$$

For many particles in a region, the same result follows from the scaling of the velocities in Eq. (2).

With both diffusion and local interactions, diffusion ($\tau_D$) dominates the annihilation time for $n>1$, while for $n<1$ the force ($\tau_F$) does. This follows directly from the particle dynamics [Eq. (2)]. Rescale all distances by $l_{AB}$, and rescale time by $l_{AB}^2$, so that diffusion is unchanged in the scaled coordinates as $l_{AB}$ increases. Scaled velocities due to the force are then multiplied by $l_{AB}^{1-n}$. As a result, forces do not asymptotically contribute for $n>1$, while forces dominate for $n<1$. For $d>2$, this leads to the initially counterintuitive result that diffusion dominates for $1<n<d-1$, even though $\tau_D \gg \tau_F$. This is a well-known result for $n=2$ [29]. Essentially, the competition between diffusion and the attractive interaction is along the separation vector between two particles, and hence is always one dimensional in character. Indeed, in $d=1$ the faster annihilation mechanism dominates, and the marginal value is $n=1$. We have confirmed these predictions for various $n$ in $d \leqslant 3$ by placing a particle and an

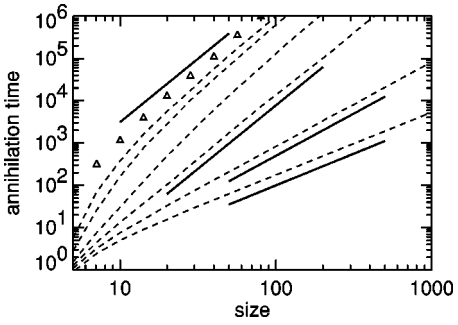


FIG. 3. Annihilation time $\tau(l)$ vs size $l$ of a particle-antiparticle pair placed in periodic boxes of size $l$ in $d=3$, where the particles are initially $l/4$ apart. They evolve according to Eq. (2) with a central force $f=1/r^n$, mobility $\eta=1$, diffusion constant $D=\frac{1}{4}$, and time step $\delta t=1$. The dashed curves correspond to, from bottom to top, $n=\frac{1}{2}$, 1, $\frac{3}{2}$, 2, 3, and 4. Triangles correspond to purely diffusive motion. The short solid lines indicate the expected asymptotic behavior, with $\tau(l)\sim l^{3/2}$, $l^2$, and $l^3$ (twice), from bottom to top, respectively. Diffusion, with $\tau_D\sim l^3$, dominates asymptotically for $n\geqslant 1$.

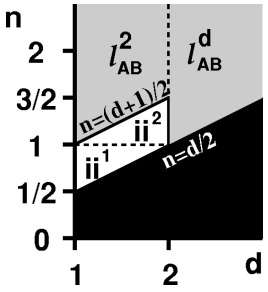


FIG. 4. Dominant annihilation times for force and noise, with uncorrelated initial conditions. Diffusive annihilation ($\tau_D$) dominates in the shaded region, while ballistic annihilation ($\tau_B \sim l_{AB}^d F^{d-2}$) dominates in the clear region. The regions [ii$^1$] and [ii$^2$] correspond to Fig. 5. For equilibrium high-temperature initial conditions, when noise is present, $\tau_D$ always dominates. For force-only annihilation, irrespective of initial conditions, $\tau_B \sim l_{AB}^d F^{(d-n-1)/n}$ dominates for $n<d$ while $\tau_F\sim l_{AB}^{n+1}$ dominates for $n>d$.

antiparticle in a periodic box, and plotting the average annihilation time as a function of the box size. In Fig. 3, we show our results for $d=3$. For $n>1$, the long-range force merely changes the effective capture size, leaving $\tau_D\sim l_{AB}^d$.

When an applied or nonlocal force $F$ is present, we must also consider ballistic annihilation. With a velocity proportional to $F$, and in a time $\tau_B$, particles sweep out a volume proportional to $\tau_B F l_*^{d-1}$, where $l_*$ is the radius of the effective capture cross section. Equating this to the typical volume $l_{AB}^d$ per particle, we obtain the typical ballistic annihilation time

$$\tau_B\sim l_{AB}^d l_*^{1-d}/F. \tag{13}$$

When no noise is present, a particle will be captured by local interactions only at separations less than $l_*$ where local interactions are as large as $F$, so that $F\sim f\sim 1/l_*^n$ or $l_*\sim F^{-1/n}$. We can use the typical forces $F(r)$ from Table I, but must evaluate them at the reaction-zone width $W$ (see below, Sec. II E)—since the reaction zone itself is neutral at a coarse-grained scale. Because $F$ depends on the system morphology, this requires a self-consistent solution [30]. The results are simple: for $n>d$ we find $l_*\gtrsim l_{AB}$ and the dominant time scale is $\tau_F$, while for $n<d$ we find $l_*\lesssim l_{AB}$, and so the dominant time scale is $\tau_B$. This corresponds to the naive phase-space result from Eq. (10) that charges from far away dominate local forces, and hence $\tau_B$ dominates, only when $n<d$.

When diffusive noise is present, we first ignore the local interactions and only consider an applied field $F$. For $d>2$, both the random walk and the ballistic force sweep out volume proportional to time. Because $F$ decreases with time, $\tau_D$ always asymptotically dominates. However, for $d\leqslant 2$, random walks recur, and the ballistic drift can enhance the volume covered by the random walk by suppressing the recurrence. The rate of volume swept out by the drifting particle, is a sphere of radius $l_*$ every $\Delta t\sim l_*/F\sim l_*^2/D$. This implies $l_*\sim 1/F$, and leads to $\tau_B\sim l_{AB}^d F^{d-2}$.

When both noise and local interactions are present, the local capture cross section $l_*$ is determined by the dominant nonballistic process—i.e., $\tau_D$ for $n>1$ and $\tau_F$ for $n<1$. The shortest annihilation time for uncorrelated initial conditions is given in Fig. 4. For equilibrated initial conditions, $\tau_D$ always dominates for $n>1$.

Our treatment of particle annihilation is essentially microscopic rather than coarse grained, since we have built the particle separation $l_{AB}$ directly into the annihilation times. We have derived our results by considering particle pairs, though we have included some multiparticle effects by never allowing particles to ''escape'' further than $l_{AB}$ from an antiparticle. We apply the results in mixed regions of the system such as reaction zones.

### D. Domain morphology: Segregated or mixed

We assume the system is described by one of two morphologies [31], depending on whether coarse-grained charge fluctuations are comparable to or much less than the mean particle density at late times. The former case describes a segregated morphology with domains of particles separate from domains of antiparticles. In the second case, there is a mixed morphology with no clearly defined domains. We can use the dominant flux $J$ and fastest annihilation time $\tau$ to see which morphology is consistent. The system turns out to have a unique consistent morphology: either mixed or segregated.

First consider a segregated morphology. The system has domains of scale $L$ separated by reaction zones of width $W$. Within the zones there is a typical particle spacing $l_{AB}$. We ignore correlations or structure within the zones [32]. Our self-consistency constraints are that $l_{AB}\gtrsim l_{AA}$, and that $W\lesssim L$. We impose the former because annihilation takes place in the reaction zone but not in the domain bulk, so the density in the reaction zone should be smaller as a result. We impose the latter since if it were not the case, with $W\gg L$, the system would be effectively *all* reaction zone and of a mixed morphology. These constrain the maximum rate that reaction zones can ''process'' incoming particles: the average density of particles that are in reaction zones, $WL^{d-1}/(l_{AB}^d L^d)$, is at

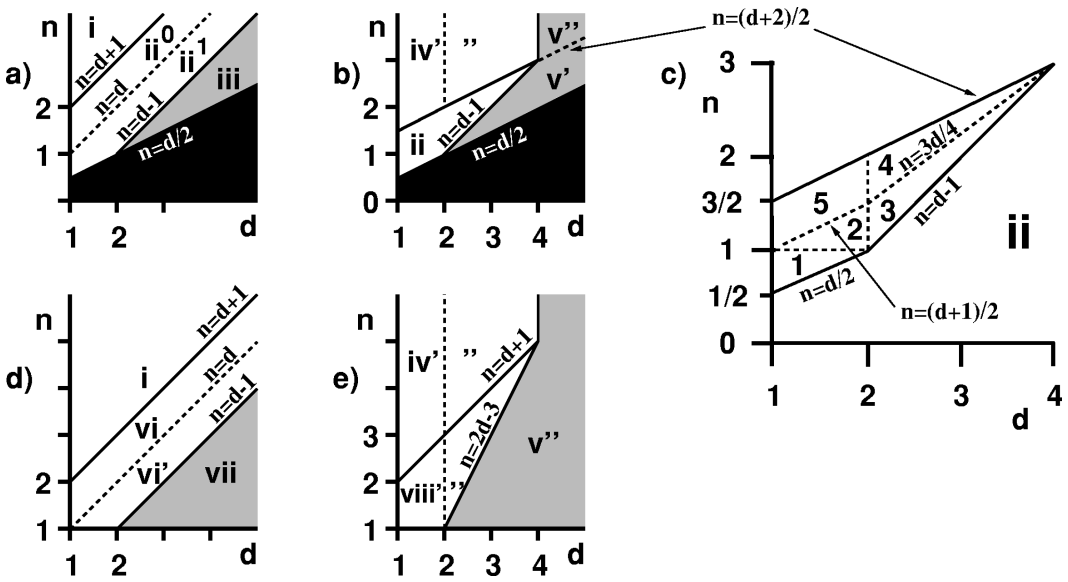


FIG. 5. Different regimes of density evolution. Blank regions indicate a segregated morphology, shaded a mixed morphology, and black excluded regimes that have no thermodynamic limit. Dashed lines separate regimes, numbered with Roman numerals, with different reaction-zone structure (see Tables II and III). The figures correspond to (a) uncorrelated initial conditions, force only; (b) uncorrelated initial conditions, diffusion and force; (c) enlargement of (b), with the $[\mathrm{ii}^1]$–$[\mathrm{ii}^5]$ subregions numbered; (d) equilibrated high-temperature initial conditions, force only; and (e) equilibrated initial conditions, noise and force.

most $1/l_{AA}^d$. Conversely, the maximum annihilation rate is $1/\tau(l_{AA})$, since $\tau(l)$ is monotonic. Combining these, the maximum annihilation rate from reaction zones is $\partial_t\overline{\rho}_{\max}\sim -1/[l_{AA}^d\tau(l_{AA})]$. For segregated systems, the actual rate of particles annihilating per unit volume is determined by the currents entering the reaction zones: $\partial_t\overline{\rho}_{\mathrm{seg}}\sim -JL^{d-1}/L^d\sim -J/L$.

If the maximum reaction rate $\partial_t\overline{\rho}_{\max}$ asymptotically dominates the actual rate $\partial_t\overline{\rho}_{\mathrm{seg}}$, then a domain structure is consistent. Indeed, since $\partial_t\rho_{\max}$ is the rate of density decrease in a mixed morphology, the inequality indicates that the background density decays quickly with respect to the charge fluctuations—i.e., that the segregated structure occurs when it is consistent. If the maximum reaction rate is less than the particle flux, then segregated domains *cannot* be sustained, and the mixed morphology should result. For the segregated morphology, we use $\partial_t\overline{\rho}\sim -J/L\sim -\overline{\rho}/t$ and $L\sim l_{AA}^{d/\mu}$ to extract the domain scale and particle density within the domain.

For the mixed morphology, the flux does not drive annihilation of the mean density. Rather, every particle is effectively in a reaction zone and has a characteristic lifetime $\tau$. Comparing this to the scaling of the density evolution, $\partial_t\overline{\rho}\sim -\overline{\rho}/t\sim -\overline{\rho}/\tau$, indicates that $\tau(l_{AA})\sim t$.

The resulting growth law regimes are shown in Fig. 5 for systems with either uncorrelated or high-temperature equilibrated initial conditions, and with either force-only or force-and-noise dynamics. The exponents are summarized in Table II. The noise-only case reproduces the Ovchinnikov-Zeldovich-Toussaint-Wilczek result [1], and is given in Fig. 5(b) by the short-range ($n\to\infty$) limit of the force-and-noise dynamics with uncorrelated initial conditions.

We can now consider the consistency of the mixed morphology. The system has no domain structure, and has local charge separation scales $l_{AB}\sim l_{AA}$. Coarse-grained charge fluctuations, above a scale $X(t)$, remain from the initial conditions. The mixed morphology is consistent if the charge density of the remaining charge fluctuations $\delta\rho(X)\sim X^{-\mu}$ is much less than the mean particle density $\overline{\rho}\sim l_{AA}^{-d}$.

Given the scaling of net currents $J(X)$, the charge fluctuations evolve with $\partial_t\delta\rho(X)\sim\delta\rho/t\sim JX^{d-1}/X^d\sim J/X$. For diffusive currents, $J_D(X)\sim\delta\rho(X)/X\sim X^{-(\mu+1)}$, and we find that $X\sim t^{1/2}$. For force driven currents, $F(X)\sim X^{d-n-\mu}$ from Eq. (10), using $X$ as the upper and lower cutoff. The force drives the net charge density $\delta\rho(X)$, and yields a net current $J_F(X)\sim X^{d-n-2\mu}$, leading to $X\sim t^{1/(\mu+n+1-d)}$. Using the results for $l_{AA}$ from above, we confirm that $\delta\rho(X)\ll\overline{\rho}$ within the mixed regions of Fig. 5.

Our exponents apply at regime boundaries, where they are continuous. However our approach does not determine any logarithmic factors. [Indeed, logarithmic factors are expected at $n=d$, whenever $J_F$ or $\tau_B$ dominates, due to the logarithmic divergence of the integral for $F$, Eq. (10).] At a boundary between mixed and segregated regimes, any logarithms present determine the dominant morphology through the self-consistent approach described above. Without logarithms, the mixed morphology applies on the boundary, since $W\sim L$ there. The width $W$ characterizes the mean-distance to annihilation for particles, and thus there is a finite density of antiparticles any finite multiple of $W$ into a domain. When $W\sim L$, there is a finite density of antiparticles arbitrarily deep within a domain—i.e., the system is mixed. This is the case in the diffusion only case at $d=4$, which mixes [2].

### E. Reaction zone

For reaction-diffusion systems with a segregated morphology, much progress has been made on the structure and evolution of the reaction zones between domains [3–7]. With

TABLE II. Growth laws of $l_{AA}$, $L$, $l_{AB}$, and $J$ for the different labeled regimes in Fig. 5. Lengths with the same scaling as $l_{AA}$ are indicated. The last column indicates the dominant flux mechanism, where $D$ is diffusive and $F$ is force driven.

| | $d\ \ln l_{AA}/d\ln t$ | $d\ \ln L/d\ln t$ | $d\ \ln l_{AB}/d\ln t$ | $-d\ \ln J/d\ln t$ | $J$ |
|---|---|---|---|---|---|
| i | $1/(n+3)$ | $2/(n+3)$ | $(n+d+1)/[(n+d)(n+3)]$ | $(n+d+1)/(n+3)$ | $F$ |
| ii$^0$ | $1/(2n+2-d)$ | $2/(2n+2-d)$ | $2n/[(n+d)(2n+2-d)]$ | $2n/(2n+2-d)$ | $F$ |
| ii$^1$ | $''$ | $''$ | $l_{AA}$ | $''$ | $F$ |
| ii$^2$ | $''$ | $''$ | $''$ | $''$ | $F$ |
| ii$^3$ | $''$ | $''$ | $''$ | $''$ | $F$ |
| ii$^4$ | $''$ | $''$ | $4n/[3d(2n+2-d)]$ | $''$ | $F$ |
| ii$^5$ | $''$ | $''$ | $2n/[(d+1)(2n+2-d)]$ | $''$ | $F$ |
| iii | $(2n+1-d)/[n(2n+2-d)]$ | $l_{AA}$ | $l_{AA}$ | $''$ | $F$ |
| iv$'$ | $\frac{1}{4}$ | $\frac{1}{2}$ | $(d+2)/[4(d+1)]$ | $(d+2)/4$ | $D$ |
| iv$''$ | $''$ | $''$ | $(d+2)/(6d)$ | $''$ | $D$ |
| v$'$ | $1/d$ | $l_{AA}$ | $l_{AA}$ | $2n/(2n+2-d)$ | $F$ |
| v$''$ | $''$ | $''$ | $''$ | $(\mu+1)/2$ | $D$ |
| vi | $(2d+1-n)/[d(n+3)]$ | $2/(n+3)$ | $2(d+1)/[(d+n)(n+3)]$ | $2(d+1)/(n+3)$ | $F$ |
| vi$'$ | $''$ | $''$ | $l_{AA}$ | $''$ | $F$ |
| vii | $(n+nd+d-1)/[nd(n+3)]$ | $l_{AA}$ | $l_{AA}$ | $''$ | $F$ |
| viii$'$ | $\mu/(2d)$ | $\frac{1}{2}$ | $(\mu+1)/[2(d+1)]$ | $(\mu+1)/2$ | $D$ |
| viii$''$ | $''$ | $''$ | $(\mu+1)/(3d)$ | $''$ | $D$ |

long-range interactions, we develop a similar approach that balances the dominant flux *into* the reaction zone with the dominant annihilation mechanism *within* the reaction zone. This balance determines the reaction zone width $W(t)$ and the interparticle spacing within the reaction zone, $l_{AB}(t)$. To simplify our discussion, we take the density of both species to be uniform throughout the reaction zone [32].

When a particle enters the reaction zone, it travels a typical distance $W$ before it annihilates—the ''annihilation mean free path.'' For a segregated system, $W$ must characterize the width of the reaction zone. A reaction zone that grows less rapidly than $W$ allows almost all particles to pass through unannihilated. On the other hand, a reaction zone that grows more rapidly than $W$ would provide an infinite number of annihilation mean free paths as $t\to\infty$, and would not have a mix of particles and antiparticles at the far edge of the reaction zone. Since slower or faster growth is not self-consistent, $W(t)$ characterizes the typical reaction-zone width.

In the annihilation time $\tau$, a particle diffuses a typical distance $W_D\sim(D\tau)^{1/2}$, or it ballistically moves $W_B\sim F\tau$ under an applied field $F$, where $F$ is given by Table I. In any case, a particle must move at least the interparticle spacing to annihilate, $W_F\sim l_{AB}$. The largest of these widths describes how far a particle travels before annihilation, and so characterizes the width of the reaction zone.

The reaction lifetime $\tau$, the particle spacing in the reaction zone $l_{AB}$, and the zone width $W$ are determined self-consistently. Given the dominant flux $J$, we equate the overall flux density into reaction zones $\dot{N}_{\rm flux}\sim JL^{d-1}/L^d$, with the rate of annihilation within the reaction zones $WL^{d-1}/[L^d l_{AB}^d\tau(l_{AB})]$. We choose the largest $W$ for the given $\tau$, and the fastest $\tau$ for the given $l_{AB}$. These dominate the width and annihilation, respectively. This provides a self-consistent solution for $\tau$, $l_{AB}$, and $W$.

For diffusion-only systems in $d\leqslant 2$, our argument is essentially that of Leyvraz and Redner [7]. We recover their results of $W\sim l_{AB}\sim t^{3/8}$, and $t^{1/3}$ in $d=1$ and 2, respectively. For $d>2$, however, we have $W\sim\sqrt{\tau_D}\sim l_{AB}^{d/2}$, since random walks are no longer space filling, and we obtain $l_{AB}\sim t^{5/18}$ and $W\sim t^{5/12}$ in $d=3$, and $l_{AB}\sim l_{AA}\sim\frac{1}{4}$ and $W\sim L\sim t^{1/2}$ in $d=4$. Our results coincide with the renormalization-group scaling results of Lee and Cardy [3]. We also recover their scaling relations with respect to currents, whenever $\tau_D$ dominates annihilation. In particular, with $\partial_t\overline{\rho}\sim J/L\sim W/(Ll_{AB}^d\tau_D)$, $\tau_D$ from Eq. (11), and $W_D\sim\sqrt{\tau_D}$, we have $W_D\sim J^{-1/3}$ and $l_{AB}\sim J^{-2/(3d)}$ for $d>2$ and $W_D\sim l_{AB}\sim J^{-1/(d+1)}$ for $d<2$. These relations hold independently of the process that dominates the currents.

Even within the mixed morphology, it is interesting to consider the distance $W$ a particle travels in a lifetime $\tau$. This distance $W(t)$ is the same scale as the remaining charge fluctuations, $X(t)$, as discussed above in Sec. II D. This is reasonable, since charge fluctuations at scales much larger than $W$ cannot be flattened out by charge motion. We summarize our results in Table III.

### F. Discussion

In all cases the density decays more slowly as $n$ increases, as the potential becomes sharper and hence shorter ranged. If noise is present, then diffusive processes eventually dominate as $n$ increases. As the spatial dimension $d$ is increased for any $n$, then a mixed morphology is eventually reached. For generalized Coulombic systems, with $n=d-1$, the density decays as $\overline{\rho}\sim 1/t$ in all combinations of high-temperature

TABLE III. Growth laws of $W$, $\tau$, and $l_*$ for the different labeled regimes in Fig. 5. Reaction-zone widths $W$ with the same scaling as $l_{AB}$ are indicated. The dominant mechanisms determining $W$ and $\tau$ are also indicated, where $D$ is diffusive, $F$ is force driven, and $B$ is ballistic. Note that when the morphology is mixed, $\tau \sim t$ and $W$ indicates the scale of remaining charge fluctuations.

| | $W$ | $d \ln W/d \ln t$ | $\tau$ | $d \ln \tau/d \ln t$ | $d \ln l_*/d \ln t$ |
|---|---|---|---|---|---|
| i | $F$ | $l_{AB}$ | $F$ | $(n+1)(n+d+1)/[(n+d)(n+3)]$ | — |
| ii$^0$ | $F$ | $l_{AB}$ | $F$ | $2n(n+1)/[(n+d)(2n+2-d)]$ | — |
| ii$^1$ | $B$ | $(d^2+2n-nd-d)/[n(2n+2-d)]$ | $B$ | $1+d(d-n-1)/[n(2n+2-d)]$ | $(2n-d)/[n(2n+2-d)]$ |
| ii$^2$ | $B$ | $(d^2+2n-2nd)/(2n+2-d)$ | $B$ | $(d^2+4n-2nd-d)/(2n+2-d)$ | $''$ |
| ii$^3$ | $B$ | $2(d-n)/(2n+2-d)$ | $D$ | $d/(2n+2-d)$ | — |
| ii$^4$ | $D$ | $2n/[3(2n+2-d)]$ | $D$ | $4n/[3(2n+2-d)]$ | — |
| ii$^5$ | $D$ | $l_{AB}$ | $D$ | $4n/[(d+1)(2n+2-d)]$ | — |
| iii | $B$ | $2/(2n+2-d)$ | $B$ | 1 | $(2n-d)/[n(2n+2-d)]$ |
| iv$'$ | $D$ | $l_{AB}$ | $D$ | $(d+2)/[2(d+1)]$ | — |
| iv$''$ | $D$ | $(d+2)/12$ | $D$ | $(d+2)/6$ | — |
| v$'$ | $B$ | $2/(2n+2-d)$ | $D$ | 1 | — |
| v$''$ | $D$ | 1/2 | $D$ | 1 | — |
| vi | $F$ | $l_{AB}$ | $F$ | $2(d+1)(n+1)/[(d+n)(n+3)]$ | — |
| vi$'$ | $B$ | $(2n+nd+1-n^2-d)/[n(n+3)]$ | $B$ | $(3n+nd+1-d)/[n(n+3)]$ | $(n+1)/[n(n+3)]$ |
| vii | $B$ | $2/(n+3)$ | $B$ | 1 | $''$ |
| viii$'$ | $D$ | $l_{AB}$ | $D$ | $(\mu+1)/(d+1)$ | — |
| viii$''$ | $D$ | $(\mu+1)/6$ | $D$ | $(\mu+1)/3$ | — |

or uncorrelated initial conditions and force and/or diffusive processes. They are always of mixed morphology.

With equilibrated initial conditions, diffusive processes dominate independently of $n$ when they are present. This is reasonable, since the high-temperature initial conditions balance the interactions with temperature. Temperature then becomes more relevant as it is reduced during the quench.

For systems without diffusive processes, the growth regimes and processes for uncorrelated and high-temperature initial conditions, in Figs. 5(a) and 5(d), respectively, correspond. The various growth exponents differ only due to the different initial charge fluctuations, characterized by $\mu$. On the other hand, with both diffusive and long-range processes the regimes do not correspond, between Figs. 5(b) and 5(e), because the competition between force and diffusive processes depends on the charge fluctuations through $\mu$.

Exponents are continuous at regime boundaries for $l_{AA}$, $l_{AB}$, $L$, $\tau$, and $W$. For segregated systems $L \gtrsim W \gtrsim l_{AB} \gtrsim l_{AA}$, where the last inequality holds since reactions should decrease the particle density. We also check that $\tau \lesssim t$ in all cases. In $d=1$, we check $W \sim l_{AB}$, as expected since the reaction zone is precisely one $AB$ pair. At the border between mixed and segregated morphologies, the reaction zone is maximal, i.e., $W \sim L$ and $l_{AB} \sim l_{AA}$.

The particle density at the edge of a domain, at $r \sim W$ in Eq. (8), scales the same as the particle density within the reaction zone, $l_{AB}^{-d}$. i.e., that $l_{AB}^{-d} \sim l_{AA}^{-d}(W/L)^{\alpha}$. Interesting special cases occur where $J_F$ dominates the flux but $W_D$ dominates the reaction-zone width (regions [ii$^4$] and [ii$^5$]). In these special cases, the singular domain profile, with $\alpha < 1$, leads to a diverging diffusion flux as the domain edge is approached, which must eventually dominate at some distance $L_X$ from the domain edge. In particular, $L_X$ is determined by $\rho(L_X)/L_X \approx J_F$. Using the domain profile [Eq. (8)], we have $L^{-\mu-\alpha} L_X^{\alpha-1} \sim J_F$. If $L_X \ll W$, then the crossover is preempted by the reaction zone and we do not expect to observe it [33]. However, precisely when $J_F$ and $W_D$ dominate we find that $W_D \ll L_X \ll L$, so that a linear transition regime is expected for $W_D \ll r \ll L_X$. The intermediate linear regime, when it occurs, does not change the density evolution or reaction-zone structure, since $J_F$ still characterizes the flux.

In reaction-diffusion systems, $d_c$ is the critical dimension above which a coarse-grained reaction rate $\lambda \rho_A \rho_B$ applies, and $d_u$ can be defined as the dimension above which we can neglect inhomogeneities. Below $d_c$ the reaction term is not given by $\rho^2$ in a coarse-grained description, and local density fluctuations must be taken into account [3,8]. Above $d_u$ we can ignore spatial gradients and have $\partial_t \overline{\rho} \sim -\overline{\rho}^2$, and hence $\overline{\rho} \sim 1/t$ (see Ref. [1]). Both of these effects stem from the diffusive annihilation mechanism. The local annihilation rate $\rho/\tau_D$ is proportional to $\rho^2$ only for $d>2$ where $\tau_D \sim \rho^{-1}$. This sets $d_c=2$. The mixed state is found for $d \geqslant 4$, so that $d_u=4$.

When only long-range interactions are included, these definitions are not as useful since neither $\tau_F$ nor $\tau_B$ are in general proportional to $\rho^{-1}$. As an example, when only force-driven evolution is included, as in Figs. 5(a) and 5(d), the density in the *mixed* state has a $d$-dependent exponent; see regions [iii] and [vii]. Even the long-wavelength charge fluctuations remain relevant to drive the dominant ballistic annihilation. We could describe this as $d_c = d_u = \infty$.

When diffusive and long-range processes are included, however, we see from Table III that the diffusive process

$\tau_D \sim l_{AB}^d$ dominates above $d_c = 2$, so that the critical dimension is unchanged from the diffusion-only case. In mixed morphologies diffusive annihilation always dominates, so that $d_u$ equals the dimension where the mixed morphology starts. For uncorrelated initial conditions we find $d_u = n+1$ for $n<3$, while $d_u = 4$ above. For high-temperature initial conditions $d_u = (n+3)/2$ for $n<5$, while $d_u = 4$ above. Since diffusive processes dominate all regimes in Fig. 5(e), it is only through the suppression of initial charge fluctuations that the long-range interactions modify $d_u$.

We have assumed that the domains of the segregated morphology are characterized only by a size $L$ and characteristic particle separation $l_{AA}$, and that the reaction zones are similarly characterized by a width $W$ and a particle separation $l_{AB}$. This leads to the exponents summarized in the tables and figures. It remains possible that other lengths enter into the asymptotic evolution, for instance through fluctuations in the shape of domain boundaries (see, e.g., Ref. [8]). Our results are most robust for $n<d$, where only the domain scale $L$ enters in the calculation of the forces and currents. Because of that, we obtain the same result for the evolving density in a segregated morphology after a coarse graining to $O(L)$, and any new but shorter lengths would not change this result. It remains possible, however, that additional lengths change the structure of the reaction zone, and hence change the boundary between segregated and mixed morphologies. Similarly, higher point correlation effects may lead to more intermediate morphologies within what we label the mixed regime. For $n>d$ additional lengths would affect the evolution of the density, since short scales enter into the calculation of the characteristic forces and currents.

Spatial fluctuations of coarse-grained quantities have also been neglected in our treatment. We *assume* that fluctuation effects are not strong enough to change our results for exponents. Another way to view fluctuations is in terms of the distribution of various quantities. We effectively assume that distributions have negligible tails.

We have also not included the motion of domain boundaries, either from local heterogeneities in domain density, or from differing mobilities of the particle species. Domain motion should not affect the scaling exponents *if* the boundaries move slowly enough for the domain profile $\alpha$ to maintain itself. A simple check is reassuring. The flux required to move domain interfaces, $J_{\rm motion} \sim \overline{\rho}\dot{L} \sim \overline{\rho}L/t$, has the same scaling behavior as the characteristic flux, $J \sim L\partial_t \overline{\rho}$. Hence domain wall motion should introduce no new scales.

## III. PREVIOUS LONG-RANGE WORK

Some of the earliest work on charged $A+B\rightarrow$ systems with long-range interactions was by Toyoki [10]. He treated uncorrelated initial conditions and force-only evolution—corresponding to Fig. 5(a). He presented a mean-field analysis of the mixed morphology, our region [iii]. By considering the mean-square force on a particle, he recovered the system-size dependence for $n<d/2$. He also initiated numerical studies of $d=2$ systems. However he used a short-scale cutoff proportional to the average particle separation $l_{AA}$ (see Sec. VII), which hampers interpretation of his results. Jang *et al.* [16] numerically studied $d=2$ systems with $n=1$, and obtained $\overline{\rho} \sim t^{-0.55}$ using a large noise amplitude, and $\overline{\rho} \sim t^{-0.90}$ using a large force amplitude. This is consistent with our results of $\overline{\rho} \sim t^{-1/2}$ and $\overline{\rho} \sim t^{-1}$ for the pure noise or pure force systems, respectively.

Ispolatov and Krapivsky [11] focused on force-only evolution in $d=1$, with a segregated morphology. They obtained results consistent with ours for $n<d$, where their assumption of a constant domain profile, with $\alpha = 0$, is valid (see Table I and Sec. VIII).

Ginzburg, Radzihovsky, and Clark [12] treated coarse-grained hydrodynamic systems with uncorrelated initial conditions and with both diffusion and long-range forces, for $n \geqslant d-1$. Our particle-based treatment can be seen as complementary to their work. We obtain the same results for density evolution, but we also obtain details about the reaction zone —including $W$, $l_{AB}$, and $\tau$. We also identify the mixed or segregated morphology of the system. Furthermore, the system-size dependence in the force for $n<d/2$ [10,11] was missed in their treatment. It would be interesting to extend their approach to include the particle nature of the charges, possibly with new phenomenological annihilation terms. Burlatsky, Ginzburg, and Clark [13] presented a simple scaling model that obtains the same results as the self-consistent approach of Ref. [12].

## IV. ELECTRONIC SYSTEMS

Asymptotic nongeminate pair recombination in clean crystalline semiconductor systems should be described by our approach with $n=2$ and equilibrated high-temperature initial conditions. In $d=3$, we find $\overline{\rho} \sim t^{-1}$ with a mixed morphology. This result applies for every combination of uncorrelated or high-temperature initial conditions. This is because *all* annihilation mechanisms have the same scaling, $\tau \sim l_{AB}^3$.

In contrast, for $d<3$ the annihilation mechanisms differ, and the morphologies are all *segregated*. The structure of the evolving charge fluctuations is thus much richer. Specifically, in $d=1$ and 2 we expect regime [viii′] to apply asymptotically with $\overline{\rho} \sim t^{-1/4}$ and $t^{-3/4}$, respectively. The decay rate is dramatically slowed due to the segregated morphology.

Clean $d=2$ systems exist in quantum Hall effect (QHE) devices. QHE devices with Skyrmion charge excitations (see, e.g., Ref. [34]) may be particularly good systems to study these effects, due to their low mobilities and slow dynamics combined with sensitive time-resolved probes of their particle density. We will develop this in more detail in a separate publication [35], paying particular attention to the scaling of the amplitudes and the resulting preasymptotic crossovers in the evolution.

## V. PARTICLELIKE TOPOLOGICAL DEFECTS

Pointlike topological defects, e.g., hedgehogs in $d=3$ or vortices in $d=2$, are found in liquid crystals and in vector $O(N)$ systems in $d=N$ dimensions. Considered pairwise, these defects have power-law interactions. Indeed, early theoretical work [10] on these systems was based on the interactions of pointlike topological defects. However the evolu-

tion of systems with pointlike topological defects is different than the dynamics of Sec. II (see, however, Ref. [36]). The order parameter field that supports topological defects provides a scale-dependent mobility to particle motion. Additionally, the mobility depends on the local environment, i.e., the interaction between defects is not a two-point particle-particle interaction. We may, however, take that as a first approximation. For $d=2$ $XY$ or nematic systems, the mobility scales logarithmically with the particle velocity, $\eta(l) \sim 1/\ln(dl/dt)$ [19]. For $d=3$ $O(3)$ or nematic systems, the mobility of hedgehogs scales as the inverse separation, $\eta(l)\sim 1/l$ [37]. In general, for $O(N)$ models in $N\geqslant 3$ dimensions, $\eta(l)\sim l^{2-N}$ [19]. High-temperature equilibrated initial conditions are appropriate for quenches in physical systems. For point defects in $d\geqslant 3$, the effective interaction is linear [10] $(n=0)$, which has not been treated in this paper. However, $d=2$ systems are within our purview.

For the $d=2$ $XY$ model, interactions between defects are logarithmic $(n=1)$. Ignoring the logarithmic mobility, and including equilibrated initial conditions [27], we have a mixed morphology with all lengths scaling the same, $l_{AA} \sim l_{AB} \sim L \sim W \sim t^{1/2}$. This is found whether or not diffusive processes are included, and indeed $\tau_D \sim \tau_B \sim \tau_F \sim l_{AB}^2$ and $J_D \sim J_F \sim L^{-3}$ for this system. The single length scale and the similarities between no noise quenches and quenches with diffusion matches the phase ordering results of the $d=2$ $XY$ model [19,38].

Two phase-ordering systems that do exhibit strong scaling violations are the $d=1$ $XY$ model [39] and the $d=2$ $O(3)$ model [40]. Both of these systems support nonsingular topological textures that have particlelike aspects. However, topological textures have an intrinsic length scale that evolves in time. Significant extensions to our approach would be necessary for these systems. We may also consider interacting topological defects in the patterned structures of driven (see, e.g., Ref. [41]) systems or of systems with competing interactions (see, e.g., Ref. [42]). To apply our approach, the long-wavelength fluctuations $(\mu)$, the interaction $(n)$, the mobility $\eta(l)$ and the nature of any noise-driven transport must be identified.

## VI. LÉVY SUPERDIFFUSION

Systems with long-range Lévy superdiffusion [43] have been used to model stirred reaction-diffusion systems. While there are no long-range interactions *per se* in these systems, superdiffusion enhances the reaction rate in a manner qualitatively similar to long-range interactions. Indeed, our methods can be applied to this case and agree with the results of Ref. [17] for the late-time evolution from uncorrelated initial conditions. We also obtain additional information about the reaction-zone structure and interface profiles for segregated morphologies. For simplicity, we only consider uncorrelated initial conditions, with $\mu=d/2$.

In the discrete formulation of Lévy flight, every particle hops a random distance $r$ along a random lattice direction with probability distribution $P(r)\propto r^{-1-\gamma}$—annihilating any antiparticles it encounters along the way. We impose $1<\gamma<2$, so that the hop distribution has a finite first moment and is normalizable. The equivalent continuum dynamics is $\partial_t \rho_k = -D|k|^{\gamma}\rho_k$, where $\gamma>1$ is required.

In time $t$, taken to be large, a particle randomly Lévy walks a distance $R\sim t^{1/\gamma}$. If $\gamma>d$, the volume bounding this walk $R^d \ll t$ and the walk is recurrent, or space filling. Conversely, if $\gamma<d$ the walk is sparse, and the particle explores a volume proportional to $t$ using its finite capture radius $r_c$. Paralleling Eq. (11), the annihilation time in a well-mixed region of the system scales as

$$\tau_L \sim \begin{cases} l_{AB}^d, & \gamma<d \\ l_{AB}^{\gamma}, & \gamma>d, \end{cases} \tag{14}$$

where the typical particle-antiparticle separation in the region is $l_{AB}$. From the Lévy flight, the net distance that the particles move before annihilating is $W\sim \tau_L^{1/\gamma}$. For space-filling walks $(\gamma>d)$ $W\sim l_{AB}$, while for sparse walks $(\gamma<d)$ $W\sim l_{AB}^{d/\gamma} \gg l_{AB}$.

For a segregated morphology, there is a typical flux density leaving domains. The flux density is most easily obtained in the discrete formulation, where it is simply the number of particles that pass through a site in each time step. From the Lévy flight distribution, a fraction $p\sim 1/x^{\gamma}$ of particles contributes to the current from a given distance $x$ away. Only particles along lattice directions contribute in a single time step, and, since $\gamma>1$, the flux is dominated by particles nearby compared to the domain scale. Hence our current is $J(r)\sim \int_0^r dy[\rho(r+y)-\rho(r-y)]/y^{\gamma}$ a distance $r$ from a domain edge, where $W \ll r \ll L$. Using the domain profile from Eq. (8), and requiring that $J(r)$ approaches a constant near the domain edge, we obtain a nonlinear profile exponent $\alpha=\gamma-1$, and $J_L \sim \overline{\rho} L^{1-\gamma}$, for the particle current.

For segregated systems, we equate the flux out of domains $\partial_t \overline{\rho} \sim JL^{d-1}/L^d \sim l_{AA}^{-(d+2\gamma)}$ to the time derivative of the charge density $l_{AA}^{-d}/t$ to obtain $l_{AA}\sim t^{1/(2\gamma)}$ and $\overline{\rho}\sim t^{-d/(2\gamma)}$. The domain size $L\sim t^{1/\gamma}$. We can also obtain the rate of particle annihilation from the reaction rate within the reaction zones, $\partial_t \overline{\rho} \sim WL^{d-1}/[L^d l_{AB}^d \tau_L]$, and compare to obtain

$$l_{AB} \sim \begin{cases} t^{(d+2\gamma-2)/[2d(2\gamma-1)]}, & \gamma<d \\ t^{(d+2\gamma-2)/[2\gamma(\gamma+d-1)]}, & \gamma>d. \end{cases} \tag{15}$$

Since particles are randomly Lévy walking before annihilation, the reaction-zone width is $W\sim l_{AB}$ for $d<\gamma$, and $W \sim l_{AB}^{d/\gamma}$ for $d>\gamma$.

The system has a segregated morphology, with $W\lesssim L \sim l_{AA}^2$, for $\gamma>d/2$. For $\gamma<d/2$ the system is mixed, and the time scale is set by the annihilation rate $\tau_L\sim t$, so that $l_{AA}\sim t^{1/d}$ and $\overline{\rho}\sim 1/t$. At $\gamma=d/2$, the marginal case between segregated and mixed morphologies, we have $W\sim L$ and $l_{AB}\sim l_{AA}$. Our results agree with those of Ref. [17]. We also obtain $\alpha$, $l_{AB}$, and $W$ characterizing the domain profile and reaction zone in segregated systems.

It is interesting that while our results are qualitatively similar to those obtained with long-range *interactions*, there is no effective interaction $n$ that recovers the growth exponents for a given Lévy exponent $\gamma$. This is in contrast to the nonequilibrium steady-state properties of the kinetic Ising model, where Lévy flights generate effective long-range interactions [44].

We may be able to apply these results to the motion of a single charged particle in a quenched random potential. This motion is subdiffusive, with $\gamma>2$ and $R\sim t^{1/\gamma}$, for potentials with sufficiently long-range correlations [45]. One loop renormalization-group calculations by Park and Deem [18] for potentials caused by quenched Coulombic ions in $d=2$ $(n=1)$, matched to the asymptotic evolution without disorder, indicate that subdiffusive behavior alone may be sufficient to describe the evolution of the quenched system. If so, then our Lévy flight results may be directly applied with the appropriate $\gamma$. However, significant questions remain, such as the appropriate microscopic annihilation mechanisms for oppositely charged particles in a quenched random potential.

## VII. LONG-RANGE CUTOFFS

It is interesting to explore quenched long-range systems numerically, but the computational burden can be large. Long-range cutoffs $L_{\rm cut}(t)$, usually on the order of the interparticle spacing, accelerate a simulation, but often at the cost of changing the physics.

Long-range cutoffs contribute in two places. The first is through the force integral driving particles fluxes, $F(r)$ in Eq. (10). Any $L_{\rm cut}\ll L(t)$ replaces the upper cutoff of the integral and changes $F(r)$ for the cases where the integral is not dominated by short scales, i.e., for $n<d+1$. If $F(r)$ is changed, the domain profile exponents $\alpha$ are also affected. The second place cutoffs enter is through the annihilation time within the reaction zone [Eq. (12)]. If the cutoff is smaller than the reaction-zone spacing, $L_{\rm cut}\ll l_{AB}(t)$, then the annihilation dynamics of $\tau_F$ is changed. Ballistic annihilation times $\tau_B$ is qualitatively changed whenever $L_{\rm cut}\ll L(t)$. Amplitudes can also be affected by cutoffs, even when growth exponents are not.

As an illustration, we consider limiting interactions to nearest neighbors. Consider uncorrelated initial conditions with no diffusion [Fig. 5(a)]. For nearest-neighbor interactions, we use $L_{\rm cut}\sim l_{AA}(r)\sim\rho(r)^{-1/d}$, the local particle spacing. Putting $L_{\rm cut}$ instead of $L$ in Eq. (10) leads to the same results as $n>d+1$ in Table I for *all* $n$. In particular, the reaction-zone profile is characterized by $\alpha=d/(n+d-1)$. The nearest-neighbor cutoff is of order $l_{AB}$ within the reaction zone, so that local force-driven annihilation dynamics, with $\tau_F$, is qualitatively unchanged. The system size cannot enter the force integral, so there is no restriction on the interaction to $n>d/2$. For a segregated morphology, regime [i] applies, while in the mixed regime [iii] does, though with $W\sim l_{AB}$ and annihilation through $\tau_F$. Comparing the particle annihilation rate $\partial_t\overline{\rho}\sim J/L$ to the maximum rate supported by reaction zones $\partial_t\overline{\rho}_{\rm max}\sim\overline{\rho}/\tau_F(l_{AA})\sim 1/l_{AA}^{n+d+1}$, we find that segregation occurs for all $d<3$. In summary, nearest-neighbor interactions only leave the evolution qualitatively unchanged for $n>d+1$. A numerical test of the effects of nearest-neighbor interactions in $d=1$ is made in Sec. VIII.

## VIII. NUMERICAL INVESTIGATION

We present some numerical results on the nontrivial domain profile exponent $\alpha$ in uncorrelated one-dimensional systems without diffusion. We also consider the effect of a cutoff $L_{\rm cut}$ limiting interactions to nearest neighbors. More results will be presented in future work [35].

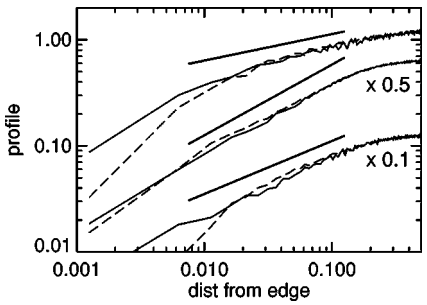


FIG. 6. Average domain profile $f(x)$ vs scaled distance $x$ from the edge of the domain. From top to bottom are $n=\frac{3}{2}$ [at $t=1.9\times10^{-5}$ (dashed) and 0.0013 (solid)], $n=\frac{3}{2}$ ($t=0.0038$ and 0.09 for dashed and solid, respectively) with nearest-neighbor interactions, and $n=2$ ($t=1.9\times10^{-5}$ and 0.25, respectively) with nearest-neighbor interactions; all are in $d=1$. The second and third sets of curves have been scaled by 0.5 and 0.1, respectively. The straight segments indicate the expected domain profiles: $\alpha=\frac{1}{4}$, $\frac{2}{3}$, and $\frac{1}{2}$. The crossover at small $x$ is due to the reaction zone, and moves to smaller scaled distance at later times.

In $d=1$, we expect $\alpha=(n-1)/2$ for $1<n<2$ (regime [ii$^0$]) and $\alpha=1/n$ for $n>2$ (regime [i]). We studied systems with 8000 particles with $n=\frac{3}{2}$ (375 samples) and $n=2$ (300 samples). We expect $\alpha=\frac{1}{4}$ and $\frac{1}{2}$, respectively. We avoided finite-size effects by comparisons with size 4000 systems. We also considered systems with only nearest-neighbor interactions, which are expected to modify the domain profile for $n<2$; see Sec. VII. In particular, we expect regime [i] to apply for *all* $n<2$. For $n=\frac{3}{2}$, we expect $\alpha=\frac{2}{3}$. We studied systems with 128 000 particles with $n=\frac{3}{2}$ (200 samples) and $n=2$ (53 samples), and checked finite-size effects with systems of 32 000 particles. We found results consistent with expectations. We show our results for the domain profiles in Fig. 6.

## IX. CONCLUSIONS

By considering the annihilation dynamics in well mixed regions of a charged-particle system, and balancing the annihilation against currents driven by charge inhomogeneities left over from the initial conditions, we self-consistently determine the morphology and evolution of quenched charged-particle systems with long-range interactions. We also contribute a visceral description of the dynamics. We characterize the system with the scale of domains $L$ and reaction zones $W$, and the particle spacings within domains $l_{AA}$ and reaction zones $l_{AB}$. For mixed systems $L\sim l_{AA}\sim l_{AB}$. Our results are summarized in Fig. 5, and in the three tables. Our primary assumption is that the lengths we have used are sufficient to characterize the evolving system. The scaling form for the domain profile [Eq. (8)] follows from this assumption.

The results of this paper will hopefully inspire more formal derivations and numerical tests, as well as experimental tests in electronic systems. Comparisons with existing treatments is encouraging, particularly agreement with the field-theory approach of Lee and Cardy [3] for reaction-diffusion systems, with the hydrodynamic treatment of Ginzburg,

Radzihovsky, and Clark [12] for uncorrelated initial conditions with diffusion and long-range interactions, and with the Lévy superdiffusion results of Ref. [17]. There are also many results pertaining to reaction zones, domain profiles, and systems with equilibrated high-temperature initial conditions.

Electronic systems ($n=2$) in two dimensions should provide an experimental test for our results. Asymptotically, we predict a segregated morphology with domain size $L\sim t^{1/2}$ and average density $\overline{\rho}\sim t^{-3/4}$ for photoexcited quantum-well or QHE systems (high-temperature equilibrium initial conditions, regime [viii′/viii″]). This will be explored at more length in a separate publication [35]. If uncorrelated initial conditions can be manufactured, then we expect regime [iv′/iv″/ii$^4$/ii$^5$] to apply: a segregated morphology with $L\sim t^{1/2}$ and $\overline{\rho}\sim t^{-1/2}$. These contrast dramatically with the mixed morphology and density decay $\overline{\rho}\sim t^{-1}$ in three-dimensional electronic systems.

## ACKNOWLEDGMENTS

I thank the EPSRC for support under Grant No. GR/J78044, the NSERC, and *le Fonds pour la Formation de Chercheurs et l'Aide à la Recherche du Québec*. I also thank John Chalker, Slava Ispolatov, Ben Lee, Klaus Oerding, Zoltan Rácz, and Beate Schmittmann for useful discussions.

[1] A. A. Ovchinnikov and Ya. B. Zeldovich, Chem. Phys. **28**, 215 (1978); D. Toussaint and F. Wilczek, J. Chem. Phys. **78**, 2642 (1983).

[2] M. Bramson and J. L. Lebowitz, J. Stat. Phys. **62**, 297 (1991); **65**, 941 (1991).

[3] B. P. Lee and J. Cardy, Phys. Rev. E **50**, R3287 (1994); J. Stat. Phys. **80**, 971 (1995); **87**, 951 (1997). Note that $\ell_{rz}\sim l_{AB}$.

[4] L. Gálfi and Z. Rácz, Phys. Rev. A **38**, 3151 (1988).

[5] S. Cornell and M. Droz, Phys. Rev. Lett. **70**, 3824 (1993).

[6] E. Ben-Naim and S. Redner, J. Phys. A **25**, L575 (1992). Note that their coarse-grained approach is only valid for $d>2$.

[7] F. Leyvraz and S. Redner, Phys. Rev. Lett. **66**, 2168 (1991); Phys. Rev. A **46**, 3132 (1992); S. Redner and F. Leyvraz, J. Stat. Phys. **65**, 1043 (1991). They impose $W\sim l_{AB}$. For reaction-diffusive systems this is correct only for $d\leqslant 2$.

[8] M. Howard and J. Cardy, J. Phys. A **28**, 3599 (1995).

[9] No diagrams dress the particle propagators of formal approaches when the only interaction is annihilation (see Ref. [3]). This is not true when long-range interactions are included.

[10] H. Toyoki, in *Dynamics of Ordering Processes in Condensed Matter*, edited by S. Komura and H. Furukawa (Plenum, New York, 1988), p. 173; Phys. Rev. A **42**, 911 (1990).

[11] I. Ispolatov and P. L. Krapivsky, Phys. Rev. E **53**, 3154 (1996). Note that their $\lambda\equiv n$.

[12] V. V. Ginzburg, L. Radzihovsky, and N. A. Clark, Phys. Rev. E **55**, 395 (1997).

[13] S. F. Burlatsky, V. V. Ginzburg, and N. A. Clark, Phys. Rev. E **54**, R1056 (1996).

[14] T. Ohtsuki, Phys. Lett. **106A**, 224 (1984). This paper applies to the generalized Coulombic model $n=d-1$, rather than $n=2$ as stated.

[15] V. V. Ginzburg, P. D. Beale, and N. A. Clark, Phys. Rev. E **52**, 2583 (1995).

[16] W. G. Jang, V. V. Ginzburg, C. D. Muzny, and N. A. Clark, Phys. Rev. E **51**, 411 (1995).

[17] G. Zumofen, J. Klafter, and M. F. Shlesinger, Phys. Rev. Lett. **77**, 2830 (1996).

[18] J.-M. Park and M. W. Deem, Phys. Rev. E (to be published).

[19] A. D. Rutenberg and A. J. Bray, Phys. Rev. E **51**, 5499 (1995).

[20] When one species is immobile correlations can become important [7], particularly for the domain structure of the immobile species. For purely diffusive systems, this is a singular limit [3].

[21] There is no pair creation, $\varnothing\rightarrow A+B$, in our dynamics. This corresponds to being at a temperature far below the chemical potential of pairs.

[22] The initial particle density is tuned by a chemical potential. It does not affect the asymptotic exponents of the subsequent evolution.

[23] P. M. Chaikin and T. C. Lubensky, *Principles of Condensed Matter Physics* (Cambridge University Press, Cambridge, 1995).

[24] M. B. Einhorn, D. L. Stein, and D. Toussaint, Phys. Rev. D **21**, 3295 (1980); C. Liu and M. Muthukumar, J. Chem. Phys. **106**, 7822 (1997).

[25] M. Mondello and N. Goldenfeld, Phys. Rev. A **42**, 5865 (1990).

[26] D. Dhar, Phys. Lett. **81A**, 19 (1981).

[27] A quenched $2D$ $XY$ model can be approximated by a system of charged-vortices interacting logarithmically, with $n=1$ (see Sec. V). Coarse-grained charge fluctuations with $\mu=2$, as described by Eq. (4), lead to the correct mixed morphology with $L\sim l_{AA}\sim t^{1/2}$ (up to logarithms; see, e.g., Refs. [19,38]). In contrast, characterizing the initial fluctuations by the excess number of vortices within a sharply defined box of size $L$, i.e., $\mu=\frac{3}{2}$, leads to a segregated morphology with $L\sim t^{1/2}$ but $l_{AA}\sim t^{3/8}$ [25], which is not observed [19,38].

[28] We coarse grain the charge density to a small but finite fraction of $L$, and we assume a smooth domain structure at that scale. Alternatively, we could build in a fractal domain structure (see Ref. [7]), but we cannot *a priori* determine if a fractal structure evolves from the dynamics.

[29] L. Onsager, Phys. Rev. **54**, 556 (1938).

[30] We self-consistently determine the shortest applicable annihilation time $\tau(l_{AB})$, the largest relevant reaction-zone width $W(\tau)$, and the corresponding particle spacing in the reaction zone $l_{AB}$, in terms of their time exponents. The results are given in Tables II and III.

[31] Other morphologies are possible in principle, though they have not been observed in reaction-diffusion systems. They would introduce new length scales.

[32] In general, reaction zones are inhomogeneous, with profiles scaled by the reaction-zone width $W$ and particle spacing $l_{AB}$ [4,6], and with dilute multiscaling tails [8]. Our analysis is

unchanged by these refinements.
[33] This linear transition zone is precisely the ''boundary layer'' in the coarse-grained treatment of Ben-Naim and Redner [6]. Note that force-driven and ballistic annihilation mechanisms, not contained in their approach, stabilize the reaction zone when $L_X \ll W$.
[34] S. E. Barrett *et al.*, Phys. Rev. Lett. **74**, 5112 (1995).
[35] A. D. Rutenberg (unpublished).
[36] The ordering kinetics of scalar systems in $d=1$ with long-range interactions reduces to alternatingly charged domain walls (particles) with long-range interactions when the domain walls are initially randomly distributed. See A. D. Rutenberg and A. J. Bray, Phys. Rev. E **50**, 1900 (1994).
[37] A. Pargellis, N. Turok, and B. Yurke, Phys. Rev. Lett. **67**, 1570 (1991); L. M. Pismen and B. Y. Rubinstein, *ibid.* **69**, 96 (1992).
[38] B. Yurke, A. N. Pargellis, T. Kovacs, and D. A. Huse, Phys. Rev. E **47**, 1525 (1993).
[39] A. D. Rutenberg and A. J. Bray, Phys. Rev. Lett. **74**, 3836 (1995).
[40] A. D. Rutenberg, W. J. Zakrzewski, and M. Zapotocky, Europhys. Lett. **39**, 49 (1997).
[41] M. C. Cross and D. I. Meiron, Phys. Rev. Lett. **75**, 2152 (1995).
[42] C. Sagui and R. C. Desai, Phys. Rev. E **52**, 2807 (1995).
[43] M. F. Shlesinger, G. M. Zaslavsky, and J. Klafter, Nature (London) **363**, 31 (1993).
[44] B. Bergersen and Z. Rácz, Phys. Rev. Lett. **67**, 3047 (1991); H.-J. Xu, B. Bergersen, and Z. Rácz, Phys. Rev. E **47**, 1520 (1993).
[45] J.-P. Bouchaud and A. Georges, Phys. Rep. **195**, 127 (1990), and references therein.